# Photocatalytic Cleavage of C–C Bond in Lignin Models under Visible Light on Mesoporous Graphitic Carbon Nitride through #-# Stacking Interaction

Huifang Liu, Hongji Li, Jianmin Lu, Shu Zeng, Min Wang, Nengchao Luo, Shutao Xu, and Feng Wang

# Photocatalytic Cleavage of C–C Bond in Lignin Models under Visible Light on Mesoporous Graphitic Carbon Nitride through π-π Stacking Interaction

*Huifang Liu [a,b], Hongji Li [a,b], Jianmin Lu [a], Shu Zeng [b,c], Min Wang [a], Nengchao Luo [a,b], Shutao Xu [c], and Feng Wang [a,] \**

[a] State Key Laboratory of Catalysis, Dalian National Laboratory for Clean Energy, Dalian Institute of Chemical Physics, Chinese Academy of Sciences, Dalian 116023, P.R. China.

[b] University of Chinese Academy of Sciences, Beijing 100049, P.R. China.

[c] National Engineering Laboratory for Methanol to Olefins, Dalian National Laboratory for Clean Energy, Dalian Institute of Chemical Physics, Chinese Academy of Sciences, Dalian 116023, P.R. China.

*Corresponding author

E-mail: wangfeng@dicp.ac.cn

**ABSTRACT**

Photocatalysis is a potentially promising approach to harvest aromatic compounds from lignin. However, the development of an active and selective solid photocatalyst is still challenging for lignin transformation under ambient conditions. We herein report a mild photocatalytic oxidative strategy for C−C bond cleavage of lignin β-O-4 and β-1 linkages using a mesoporous graphitic carbon nitride catalyst. Identifications by solid-state NMR techniques and DFT calculations indicate that π-π stacking interactions are most likely present between the flexible carbon nitride surface and lignin model molecule. Besides, low charge recombination efficiency and high specific surface area ($206.5 \ m^2 \ g^{-1}$) of the catalyst also contribute to its high catalytic activity. Mechanistic investigations reveal that photogenerated holes, as the main active species, trigger the oxidation and C–C bond cleavage of lignin models. This study sheds light on the interaction between complex lignin structures and the catalyst surface, and provides a new strategy of photocatalytic cleavage of lignin models with heterogeneous photocatalysts.

**KEYWORDS**: lignin model, photocatalysis, C–C bond cleavage, mesoporous carbon nitride, visible-light

## INTRODUCTION

Lignin, as a kind of sustainable aromatic polymers in nature, can provide high value-added aromatic chemicals or fuels as an alternative to fossil resources.[1-7] The interlinkages of lignin mainly include C−O bonds and C−C bonds. Despite some progress has been made in the transformation and fragmentation of lignin through C−O bond cleavage to aromatic monomers,[8-15] catalytic activity and selectivity should be further increased toward C−C bond cleavage.[16-22] However, the bond dissociation energies of C−C bonds in lignin are generally higher than that of C−O bonds.[23-24] And the C−C bonds reside between bulky aromatic groups, which brings the cleavage difficulty of lignin linkages on the solid surface under ambient condition due to the inefficient activation. That is the reason why most excellent results in the oxidative lignin valorization involve homogeneous metal complexes.[18] But the product separation and recycling of homogeneous catalysts can be difficult. Therefore, studies and fundamental understanding on the C−C bond cleavage of lignin models like the most common β-O-4 linkages with heterogeneous catalysts are desirable for the lignin conversion.

Photocatalysis has been recently reported to be a potentially promising approach to harvest aromatic compounds from lignin. For example, a two-step oxidation-reduction strategy has been developed for the reaction of lignin β-O-4 models through C−O bond cleavage by photoredox and Ir (Pd) catalysis.[25-26] This process has also been achieved using heterogeneous catalysts like $ZnIn_2S_4$[27-28] or a carbazolic porous organic framework.[29] In addition, photocatalytic C−C bond cleavage in one step is also a fascinating strategy for lignin conversion. For instance, the photochemical oxidation of lignin models using benzoquinone and copper achieved the C−C bond cleavage, but with only 14−62% total yields of the cleaved products.[30] Besides, it has been reported that homogeneous vanadium catalysts are active for C−C bond cleavage of β-O-4

linkages under visible light[31-32], while difficulties associated with separation and recycling still exist. Based on our previous work about the photocatalytic oxidation of β-1 linkages by CuO$_x$/ceria/anatase nanotube[33], we want to develop new strategies toward C−C bond cleavage of lignin β-O-4 models using an active solid photocatalyst and to study the interaction between a complex substrate molecule and the catalyst surface.

Graphitic carbon nitride (g-C$_3$N$_4$), a visible-light-responsive and metal-free semiconductor, has been extensively studied in environmental remediation and many organic reactions with solar energy.[34-36] Properties of large surface area, low-cost, visible light adsorption, and plenty of nitrogen atoms or vacancies, make g-C$_3$N$_4$ one of the most promising catalysts for visible-light photoredox catalysis.[37-41] As for the heterogeneously catalytic conversion of lignin models, adsorption of the molecule with bulky benzene rings on a rigid catalyst surface may need to overcome high energy barrier due to the structural complexity and large steric hindrance, while the flexible organo 2D character of g-C$_3$N$_4$[42] may provide an ideal surface here. This brings out a critical issue of substrate-catalyst interaction. Incidentally, the specific interaction between g-C$_3$N$_4$ and a complex aromatic molecule with lignin linkages has not been studied previously.

In the present work, we report an oxidative method that cleaves C−C bond in lignin models with β-O-4 or β-1 linkages under visible light by using a mesoporous graphitic carbon nitride (mpg-C$_3$N$_4$). Lignin models with two benzene rings and methoxy substituents were oxidized to aromatic oxygenates with molecular oxygen at room temperature. Photogenerated holes were demonstrated to be the main active species for this transformation. Possible interactions between a substrate molecule and flexible C$_3$N$_4$ surface were studied using solid-state NMR techniques and the adsorption patterns were explored with DFT calculations.

**EXPERIMENTAL SECTION**

**Chemicals and reagents**

Urea (AR), melamine (99%), $Bi(NO_3)_3 \cdot 5H_2O$ (> 98%), $Na_2WO_4 \cdot 2H_2O$ (99.5%), tetraethyl orthosilicate (TEOS, 99.0%) and hydrofluoric acid (HF, AR, ≥ 40%) were purchased from Aladdin Chemicals. Ethanol (AR), acetonitrile (AR), acetone (AR) and dichloroethane (AR) were purchased from Sinopharm Chemical Reagent Co., Ltd. Hydrochloric acid (HCl, 36%−38%) and nitric acid ($HNO_3$, AR) were from Tianjin Kemiou Chemical Reagent Co., Ltd. $O_2$ (99.9%) and Ar (99.9%) were obtained from Dalian Institute of Chemical Physics. A Synergy UV system from Millipore was used to deionize the distilled water (18 mΩ).

**Preparation of $C_3N_4$ catalysts**

The mesoporous graphitic carbon nitride was synthesized according to a modified method in previous work.[43] Briefly, urea (10 g) was dissolved in a solution of 0.2 M HCl solution (15 mL) and ethanol (13 mL) under stirring. And tetraethyl orthosilicate (TEOS, 8 mL) was then slowly added dropwise to the above solution. After stirring vigorously at room temperature for 3 h, the mixture was heated on a plate for the solvent evaporation and then dried at 100 °C for 10 h. The obtained white solid was calcined in a muffle furnace at 550 °C for 4 h (heating rate: 2.5 °C/min). Subsequently, hydrofluoric acid was used to remove $SiO_2$ through stirring with the above material for 20 h. Then after the following filtration, water and ethanol washing for several times, and drying at 80 °C for 12 h, the pale-yellow solid was finally obtained and denoted as mpg-$C_3N_4$.

For comparison, urea (10 g) was directly heated at 550 °C for 4 h (the same heating rate: 2.5 °C/min) in the muffle furnace, giving a pale-yellow solid denoted as $C_3N_4$-U. Similarly,

melamine as the precursor was directly heated through the same procedures, giving a yellow sample denoted as $C_3N_4$-M.

**Preparation of other semiconductors**

Semiconductors like $TiO_2$-A (Anatase-$TiO_2$, 99.8% metals basis, 40 nm, Aladdin Chemicals) and P25 (Degussa, 20 nm) were obtained commercially and directly used without further treatment in this work. $Bi_2WO_6$ was synthesized according to the literature report.[44] The general procedures are as follows: Firstly, $Bi(NO_3)_3 \cdot 5H_2O$ (2 mmol, 0.97 g) was dissolved in 1.0 M $HNO_3$ aqueous solution (15 mL), and $Na_2WO_4 \cdot 2H_2O$ (1 mmol, 0.33 g) was dissolved in 15 mL of $H_2O$. Then, the $Na_2WO_4$ solution was added into the $Bi(NO_3)_3$ solution and stirred for 30 min, after which the mixture was transferred to a 50 mL autoclave and heated at 180 °C for 24 h in an oven. After the hydrothermal crystallization process, the mixture was filtered, washed with deionized water for several times and dried at 100 °C for 12 h, giving the final solid $Bi_2WO_6$ sample.

**General characterizations**

$N_2$ adsorption and desorption of the $C_3N_4$ catalysts were measured on a Quadrasorb SI instrument (Quantachrome, USA) at 77.3 K. Nitrogen and hydrogen contents were determined through elemental analyses on a HORIBA EMGA-930 analyzer, and carbon content analysis was performed on a HORIBA EMIA analyzer. Fourier transform infrared spectra (FTIR) were collected on a Bruker Tensor 27 instrument. Powder X-ray diffraction patterns were obtained on a PANalytical X-Pert PRO diffractometer using Cu K$\alpha$ radiation at 40 kV and 20 mA, with continuous scans in a 2$\theta$ range of 5−80°. The morphology of mpg-$C_3N_4$ was examined by scanning electron microscopy (SEM, JSM-7800F) and transmission electron microscopy (TEM, JEM-2100). UV-Vis diffuse reflectance spectra of the $C_3N_4$ catalysts were recorded on a

SHIMADZU UV-2600 Spectrophotometer. Photoluminescence (PL) measurements were performed on a Fluorescence Spectrophotometer (Photon Technology International, QM 400) with the excitation wavelength at 375 nm.

**Photocatalytic reactions**

Typical reactions in this work were carried out in a homemade quartz tube under 455 nm LED light with a total power of 6 W. Typically, 0.05 mmol of lignin model, 10 mg of catalyst and 1 mL of solvent (generally $CH_3CN$, unless other solvents stated in the text) were firstly added into the reactor. And the required gas (Ar or $O_2$) was charged in, after which the tube was sealed and placed under light illumination. The reaction mixture was stirred for a desired time, with the air conditioning cooling the photocatalytic system. *CAUTIOUS! Wearing eye goggle of shielding 455 nm light is mandatory*. After reaction, *p*-methylacetophenone was added into the reaction mixture as an analytical internal standard. Then after filtering through a 0.22 μm filter, the liquid sample was diluted and analyzed by gas chromatography-mass spectrometry (GC-MS) and high performance liquid chromatography (HPLC). Conditions of gas chromatography: instruments: Agilent 7890A/5975C, HP-5 column; carrier gas: helium; split injection; inlet temperature: 260 °C; temperature program: 80~270 °C 10 °C/min, 270 °C isothermal 2 min; mass spectrometer: quadrupole detector. Conditions of HPLC: instruments: Agilent 1260 Infinity; injection: 10 μL; mobile phase: acetonitrile/water (v/v of 40/60~60/40); flow rate: 1.0 mL/min; column: Agilent Eclipse Zorbax C18 column; TCC temperature: 35 °C; detector: UV 230 nm.

Operations and results of a large-scale photocatalytic experiment using a xenon lamp are attached in the Supporting Information.

**Solid-state NMR**

A spectrometer (Bruker Avance III 600) equipped with a 14.1 T wide-bore magnet was used here for all the solid-state magic angle spinning (MAS) NMR experiments. The resonance frequencies for $^1$H, $^{13}$C were 600.1 and 150.9 MHz, respectively. For the $^1$H NMR experiments, a 4 mm H-X WVT probe was used with a spinning rate of 12 kHz, and the spin echo pulse sequence with a $\pi/2$ pulse length of 4.35 μs and $\pi$ pulse length of 8.7 μs were used. Both the $^1$H-$^{13}$C CP/MAS and heteronuclear correlation (HETCOR) experiments were performed with a spinning rate of 12 kHz. A recycle delay of 2 s and a contact time of 1 ms were recorded in $^1$H-$^{13}$C CP/MAS NMR spectra. For the two-dimensional (2D) $^1$H-$^{13}$C HETCOR NMR experiment, the increment interval was set to 41.67 μs in the indirect dimension. Typically, 256 scans were acquired for each t1 increment, and two-dimensional data sets consisted of 256 t1 × 2048. A $^1$H rf field of 57.5 kHz, a $^{13}$C rf field of 33.5 kHz, and a contact time of 1 ms were set to the sequence. The $^1$H and $^{13}$C chemical shifts were both referenced to adamantane at 1.74 ppm and the upfield methine peak at 29.5 ppm, respectively. $^1$H double quantum (DQ) NMR spectra were recorded on a 3.2 mm H-X-Y WVT probe with a spinning rate of 15 kHz using a double resonance mode. Following the general scheme of 2D multiple-quantum spectroscopy, $^1$H-$^1$H DQ coherences were excited and reconverted with a POST-C7 pulse sequence. And for each of the 128 experiments, the spectra were acquired using 16 scans with t1 increment of 33.33 μs.

**DFT calculation settings**

We used the Vienna Ab Initio Simulation Package (VASP)[45-46] for all the DFT calculations within the generalized gradient approximation (GGA) using the PBE[47] functional formulation. Projected augmented wave (PAW) pseudopotentials describe the interactions between ionic cores and valence electrons.[48-49] 1 (H), 4 (C), 5 (N), and 6 (O) valence electrons were explicitly

taken into account. Plane wave basis set with a kinetic energy cutoff of 400 eV was included. Partial occupancies of electronic bands were allowed with the Gaussian smearing method and a width of 0.10 eV. Brillouin zone integration was performed using a $6 \times 6 \times 1$ Monkhorst-Pack grid for the periodic slab with one single-layered planar g-C$_3$N$_4$ sheet and a 20 Å vacuum between the sheet and its periodic images; and a $3 \times 3 \times 1$ Monkhorst-Pack grid for the slab with a single-layered corrugated g-C$_3$N$_4$ sheet and a 20 Å vacuum. The convergence criterion for the electronic self-consistent cycles was set to $10^{-7}$ eV and that for geometry optimization was $10^{-6}$ eV.

## RESULTS AND DISCUSSION

### Photocatalytic reaction of 2-Phenoxy-1-phenylethanol

As a representative of lignin β-O-4 linkage, 2-Phenoxy-1-phenylethanol (**1**) with C$_\alpha$–OH, C$_\alpha$–C$_\beta$ and C$_\beta$–O bonds was initially used as a model substrate in this work. Other studies have reported that the oxidized products of **1** generally include a ketone (**2**) via C$_\alpha$–H oxidation and the degraded products (**3-6**) through C$_\alpha$–C$_\beta$ or C$_\beta$–O bond cleavage (Scheme 1).[17, 21, 26, 30, 50-51]
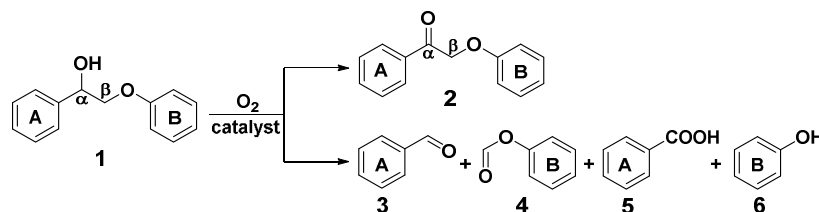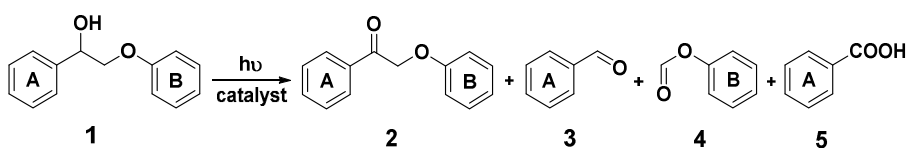


**Scheme 1.** General oxidative products of 2-phenoxy-1-phenylethanol (**1**)

To test the photocatalytic reaction of model **1**, various semiconductors have been used as the catalysts. Results with different catalysts under various conditions are summarized in Table 1. The reaction did not occur without a catalyst (Table 1, entry 1). Typical photocatalysts like TiO$_2$-A, P25 and Bi$_2$WO$_6$ showed low activity (conversions of 10−28%) for this reaction (Table 1, entries 2−4). The most common g-C$_3$N$_4$ prepared from melamine (C$_3$N$_4$-M) exhibited

relatively higher activity, with a 46% conversion and 63% C−C cleavage selectivity (Table 1, entry 5). As different precursors and preparation methods of g-$C_3N_4$ would greatly affect their catalytic activity, two other g-$C_3N_4$ samples ($C_3N_4$-U and mpg-$C_3N_4$) have also been synthesized and tested in the reaction. Herein, $C_3N_4$-U prepared from urea (Table 1, entry 6) was more active than $C_3N_4$-M with the conversion of 67% and C−C cleavage selectivity of 81%, which can be attributed to the faster carrier transport and higher surface area of $C_3N_4$-U[52]. When mpg-$C_3N_4$ was used (Table 1, entry 7), substrate **1** was nearly completely transformed with a relatively high selectivity (91%) of C−C bond cleaved products, including benzaldehyde (**3**), phenyl formate (**4**) and benzoic acid (**5**).

**Table 1.** Photocatalytic transformation of model **1** under various reaction conditions [a]



| Entry | Catalyst | Conversion (%) | Yield (%) [b] | | | | C–C cleavage selectivity (%) [c] |
|-------|----------|----------------|-----|-----|-----|-----|----------------------------------|
| | | | **2** | **3** | **4** | **5** | |
| 1 | None | 0 | - | - | - | - | - |
| 2 | $TiO_2$-A | 12 | 1 | - | - | - | - |
| 3 | P25 | 28 | 8 | 19 | 9 | - | 70 |
| 4 | $Bi_2WO_6$ | 10 | - | - | - | - | - |
| 5 | $C_3N_4$-M | 46 | 11 | 18 | 17 | - | 63 |
| 6 | $C_3N_4$-U | 67 | 10 | 20 | 17 | 25 | 81 |
| 7 | mpg-$C_3N_4$ | 96 | 7 | 51 | 30 | 21 | 91 |
| 8 [d] | mpg-$C_3N_4$ | 8 | - | - | - | - | - |
| 9 [e] | mpg-$C_3N_4$ | 5 | - | - | - | - | - |
| 10 [f] | mpg-$C_3N_4$ | 27 | 6 | 14 | 15 | 8[i] | 78 |
| 11 [g] | mpg-$C_3N_4$ | 79 | 29 | 16 | 18 | 15 | 52 |
| 12 [h] | mpg-$C_3N_4$ | 86 | 13 | 45 | 20 | 18 | 83 |

[a] Standard reaction conditions: 0.05 mmol of substrate **1**, 10 mg of catalyst, 1 mL of $CH_3CN$, 455 nm LED (6 W), $O_2$ (1 atm), 10 h. [b] GC yield of **2−5** (%) = $\frac{\text{moles of product } \textbf{2-5} \text{ formed}}{\text{moles of substrate } \textbf{1} \text{ input}} \times 100\%$. [c] C−C bond cleavage selectivity was presented as the molar ratio of (**3**+**5**)/(**2**+**3**+**5**) in product distribution. [d] Reaction conducted in the dark. [e] Reaction under 1 atm of argon. [f] Reaction in $C_2H_5OH$. [g] Reaction in $C_2H_4Cl_2$. [h] Reaction in acetone. [i] Yield of ethyl benzoate. "-" means not detected.

The reaction is photo-driven and light irradiation is necessary for this transformation, as the reaction did not occur under dark conditions (Table 1, entry 8). Besides, no product was detected under argon (Ar) atmosphere (Table 1, entry 9) with a significantly decreased conversion (5%), indicating that $O_2$ is indispensable for this reaction. In addition, solvents also have great effects on the catalytic performance. Ethanol was not a suitable solvent for this transformation with a low conversion of 27% (Table 1, entry 10). Reactions in $C_2H_4Cl_2$ and acetone showed medium conversions of 79% and 86% (Table 1, entries 11−12), respectively. Acetonitrile was the best solvent in this study, with a nearly total conversion of the substrate and a 91% selectivity of C−C bond cleavage (entry 7).

**Characterizations of $C_3N_4$ catalysts**

**Table 2.** Structural properties and compositions of the as-prepared $C_3N_4$ catalysts

| Sample | $S_{BET}$ $(m^2\ g^{-1})$ [a] | $V_{pore}$ $(cm^3\ g^{-1})$ | $d_{pore}$ (nm) [b] | C (wt %) | N (wt %) | H (wt %) | C/N atomic ratio |
|---|---|---|---|---|---|---|---|
| $C_3N_4$-M | 6.6 | 0.04 | 2.7 | 32.13 | 62.95 | 1.81 | 0.60 |
| $C_3N_4$-U | 48.2 | 0.15 | 2.9 | 28.13 | 57.16 | 1.87 | 0.57 |
| mpg-$C_3N_4$ | 206.5 | 0.42 | 3.6 | 26.11 | 56.57 | 2.33 | 0.54 |

[a] Multipoint BET surface area. [b] Average pore width determined by the DFT method.

Table 2 shows the physicochemical properties and elemental compositions of the as-prepared $C_3N_4$ catalysts. According to the $N_2$ physical adsorption results (Figure S1), the BET specific surface area of $C_3N_4$-M is only 6.6 m$^2$ g$^{-1}$, while it is 48.2 m$^2$ g$^{-1}$ for $C_3N_4$-U, indicating that precursor types affect the structure of polymeric graphitic $C_3N_4$ materials. Meanwhile, mpg-$C_3N_4$ has a much higher surface area (206.5 m$^2$ g$^{-1}$) and is verified to be mesoporous with the average pore size of 3.6 nm. From the elemental analysis, the presence of hydrogen in $C_3N_4$ materials (1.81–2.33 wt %) means the incomplete condensation of precursors leaving NH$_x$ groups remained in the catalysts. And for the mpg-$C_3N_4$, residual trace silica in the catalyst can also enhance the charge separation of electron-hole pairs[53].
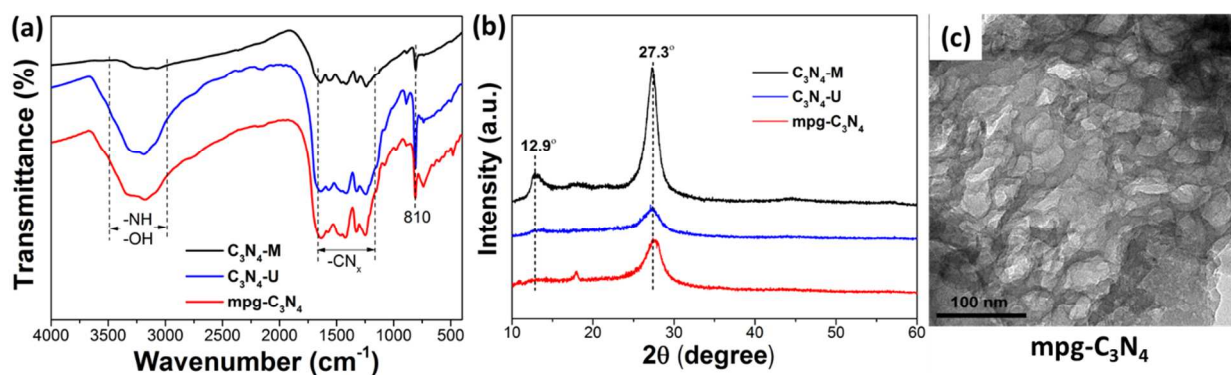


**Figure 1.** (**a**) FTIR spectra and (**b**) XRD patterns of the as-prepared $C_3N_4$ catalysts. (**c**) HRTEM image of the mpg-$C_3N_4$ catalyst.

FTIR spectra (Figure 1a) exhibit typical characters of molecular structure of $C_3N_4$ materials for all three as-synthesized catalysts.[54-55] We can see the sharp peak at 810 cm$^{-1}$ and strong bands in the 1200−1650 cm$^{-1}$ region, which are assigned to the breathing mode of tri-s-triazine units and the stretching vibration modes of C-N heterocycles, respectively. Besides, broad peaks in the region of 3000−3500 cm$^{-1}$ are ascribed to −NH$_x$ and –OH residues caused by precursors or air exposure.

In general, two typical diffraction peaks at 12.9° and 27.3° are shown in the XRD patterns (Figure 1b) of the as-prepared $C_3N_4$ catalysts, corresponding to the intralayer long-range order and interlayer periodic stacking controlled by van der Waals forces, respectively.[56] $C_3N_4$-U and mpg-$C_3N_4$ have a much weaker peak at 12.9° than $C_3N_4$-M, indicating that $C_3N_4$ synthesized from urea has less intralayer hydrogen bonds. A previous report has indicated that carbon nitride with less hydrogen bonds may show superior photoactivity because of the fast charge transfer between interlayers.[52] Besides, the relatively weak and broadened peaks at 27.3° of $C_3N_4$-U and mpg-$C_3N_4$ indicate that polymerization of urea gives the $C_3N_4$ structure with less layers. Moreover, the layer-stacked structure of mpg-$C_3N_4$ with slit pores is further clearly evidenced by the high resolution transmission electron microscopy image of it (Figure 1c and Figure S2).
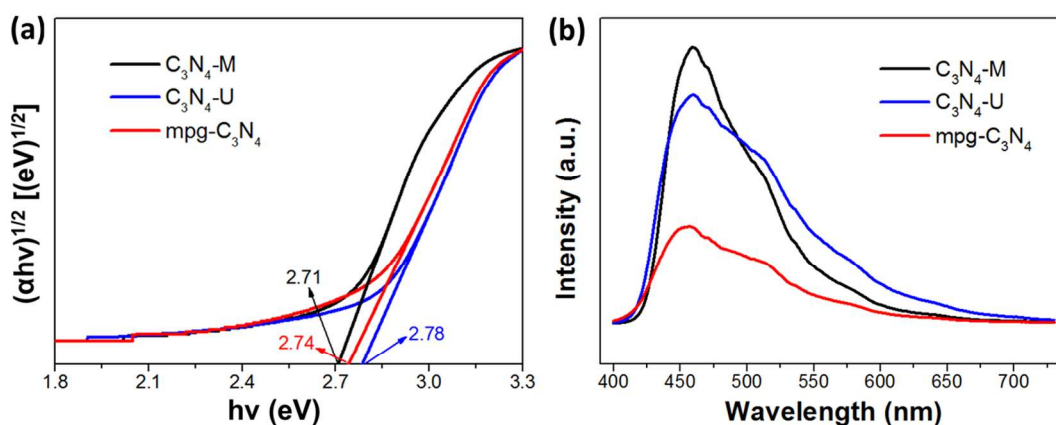


**Figure 2.** The plots of $(\alpha h\upsilon)^{1/2}$ versus photon energy (**a**) and photoluminescence spectra (**b**) of the as-prepared $C_3N_4$ catalysts.

Moreover, UV-Vis absorption and photoluminescence spectra of these $C_3N_4$ catalysts were also performed to study their optical properties. The band gaps of $C_3N_4$-M, $C_3N_4$-U and mpg-$C_3N_4$ are calculated to be 2.71, 2.78 and 2.74 eV via Kubelka-Munk plot (Figure 2a), respectively. Thus the similar light absorption of these $C_3N_4$ samples contributes little to the

activity difference among them. On the other hand, compared to $C_3N_4$-M and $C_3N_4$-U, mpg-$C_3N_4$ has a much lower photoluminescence intensity (Figure 2b), meaning that mpg-$C_3N_4$ has the lowest electron-hole recombination efficiency among them. Therefore, large surface area and low charge recombination efficiency from the introduced mesopores may contribute to the high activity of mpg-$C_3N_4$ in this photocatalytic reaction.

**Surface interaction and DFT calculations**

The substrate-catalyst interaction is a key point for heterogeneous reactions. For the carbon nitride polymer, there are different types of nitrogen functionalities in its periodic structure, which can act as the Lewis basic sites to anchor certain groups of the substrate molecule.[57] Besides, the layered conjugate structure of $C_3N_4$ can also contribute to the coplanar interaction with the reactants such as π-π stacking or other noncovalent bonds.[58]
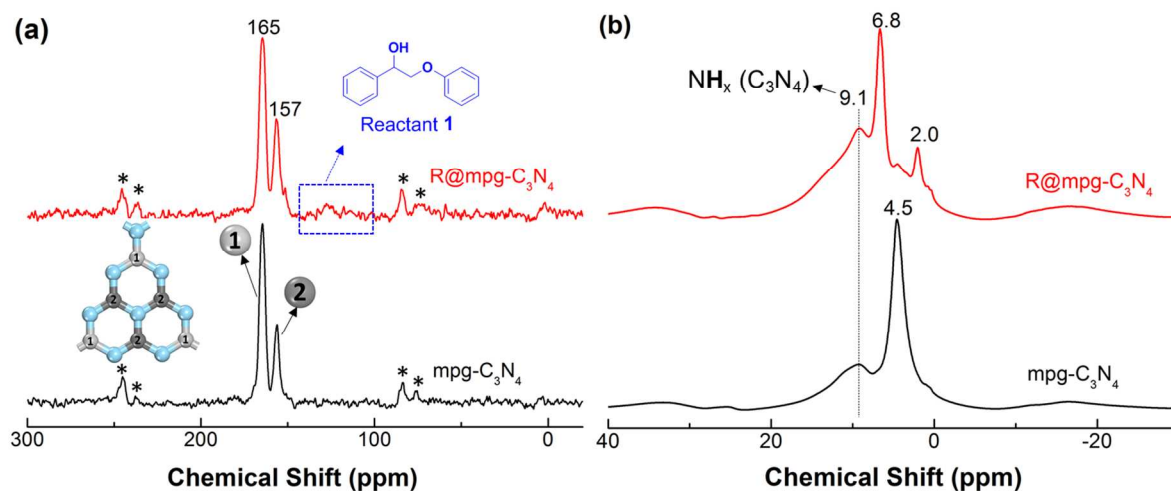


**Figure 3.** (**a**) Solid-state $^1$H-$^{13}$C CP/MAS NMR spectra and (**b**) $^1$H MAS NMR spectra of mpg-$C_3N_4$ and R@mpg-$C_3N_4$. (* denotes spinning side band. R@mpg-$C_3N_4$ was prepared as follows: 200 mg of mpg-$C_3N_4$ was dispersed in an acetonitrile solution containing 10 mg of reactant **1**, and the solvent was evaporated to obtain the dried solid R@mpg-$C_3N_4$.)

To clarify their structures and interactions between lignin model molecule and the surface of mpg-$C_3N_4$, solid-state MAS NMR experiments were conducted, with the results shown in Figure 3. In the 1D $^1H$-$^{13}C$ MAS NMR spectra (Figure 3a), only two typical carbon signals for mpg-$C_3N_4$ are observed with the peak maxima at 165 and 157 ppm, which are assigned to $CN_2(NH_x)$ and $CN_3$ moieties[59-60] respectively in $C_3N_4$. For R@mpg-$C_3N_4$ in Figure 3a, other weak signals in the blue frame correspond to aromatic carbon signals of reactant **1**. Besides, from the $^1H$ MAS NMR spectra (Figure 3b), we can see an apparent peak at 4.5 ppm and a broad peak at 9.1 ppm for mpg-$C_3N_4$, with the former assigned to the adsorbed $H_2O$ molecules on $C_3N_4$. Also in the 2D $^1H$-$^{13}C$ HECTOR MAS NMR spectrum of R@mpg-$C_3N_4$ (Figure S3), one cross signal at (165, 9.1) ppm indicates that hydrogens at 9.1 ppm are only in close proximity to the carbon at 165 ppm, which simultaneously demonstrates that peak at 9.1 ppm is assigned to $NH_x$ groups on mpg-$C_3N_4$. Moreover, a new signal at 6.8 ppm for R@mpg-$C_3N_4$ corresponds to hydrogens on the benzene rings of reactant **1** (Figure 3b). In comparison with the liquid $^1H$ NMR spectra of compound **1** (see the spectra in SI), peaks of phenyl hydrogen atoms at 7.2~7.5 ppm are not prominent, which might come from some chemical shift change due to diamagnetic anisotropy or the overlap with broad peaks at ~9.1 ppm. In addition, another small signal at ca. 2.0 ppm in Figure 3b is due to a small amount of residual acetonitrile solvent.

2D $^1H$-$^1H$ DQ MAS NMR spectroscopy was further used here to study the proton-proton proximities (< 5 Å) / interactions of the reactant molecule and the catalyst surface.[61] As shown in Figure 4, the 2D $^1H$-$^1H$ DQ MAS NMR spectrum of R@mpg-$C_3N_4$ shows three diagonal peaks at (1.9, 3.8), (6.8, 13.6) and (9.1, 18.2) ppm due to the autocorrelation of –$CH_3$ from solvent, benzene ring hydrogens from reactant **1** and $NH_x$ from mpg-$C_3N_4$, respectively. Another off-diagonal peak pair at (6.8, 15.9) ppm is also observable, indicating that aromatic hydrogens

of reactant **1** (6.8 ppm) are in close spatial proximity to the $NH_x$ groups (9.1 ppm) on mpg-$C_3N_4$.

This spatial proximity between the reactant molecule and catalyst surface may promote the transfer of photogenerated holes during the transformation,[62] which is important for photocatalytic reactions.
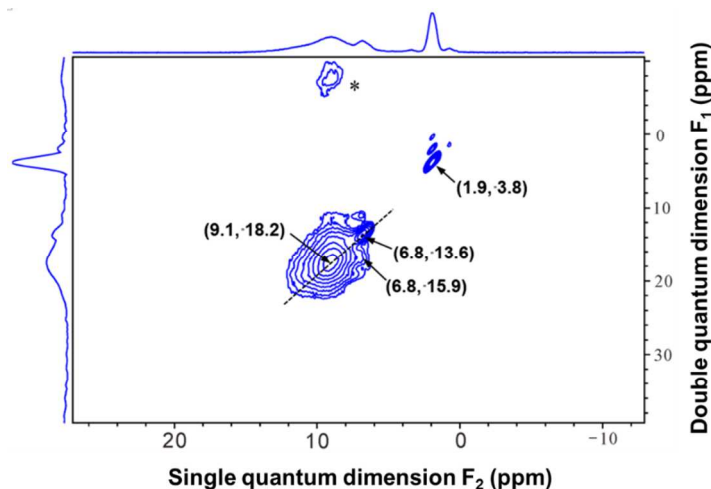


**Figure 4.** 2D $^1H$-$^1H$ DQ MAS NMR spectrum of R@mpg-$C_3N_4$ (* denotes spinning side band).

Further, we explored the interaction model between $C_3N_4$ surface and reactant molecule **1** using DFT calculations. Firstly, calculated results show that a corrugated surface is much more stable with the potential energy of 3.29 eV lower than that of a planar surface of the $2 \times 2$ $C_3N_4$ sheet (Figure S4), which is in accordance with previous report.[63] Then structures of a corrugated $4 \times 4$ $C_3N_4$ sheet with different conformations were optimized and we found that the energy differences between them (0.77 eV and 1.12 eV) were about one order less than the energy difference between the corrugated and planar $4 \times 4$ $C_3N_4$ sheet (Figure S5 and discussion in the supporting information). Therefore, conformational changes of a corrugated $C_3N_4$ surface might be flexible and geometrically beneficial for the accommodation of complex biomass molecules.
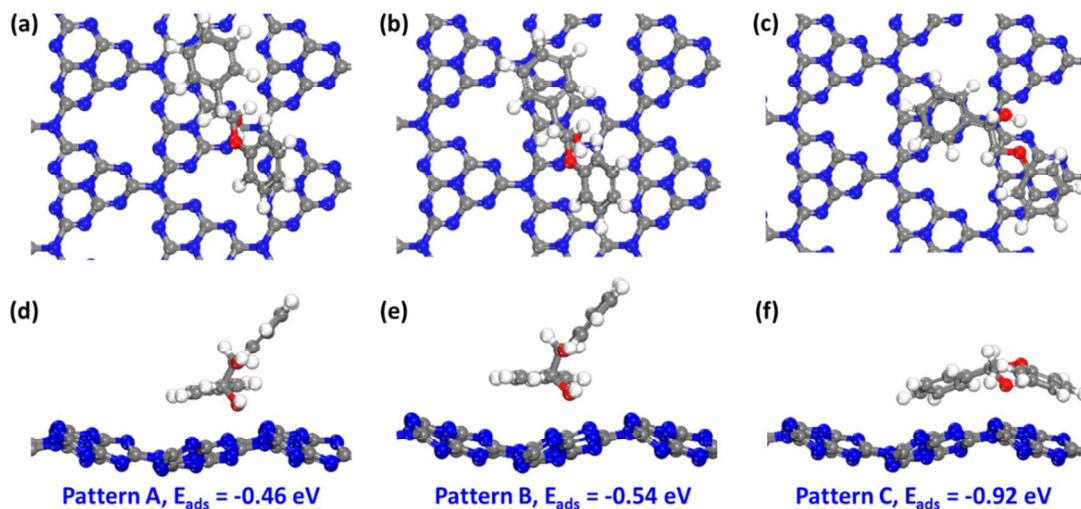
**Figure 5.** Optimized interaction patterns (top view and side view) and adsorption energies of substrate molecule **1** adsorbed on a corrugated $C_3N_4$ surface. (**a** and **d** for adsorption pattern **A**; **b** and **e** for pattern **B**; **c** and **f** for pattern **C**. Color scheme: H, white; C, gray; N, blue; O, red.)

Moreover, we have calculated possible interaction models (Figure 5) between the substrate molecule **1** and a corrugated $C_3N_4$ surface. Interaction patterns **A** and **B** correspond to the oxygen atom in OH group of molecule **1** approaching different carbon atoms in tri-s-triazine cavity (also the H atom in OH group of molecule **1** approaching N atoms in $C_3N_4$), and have similar adsorption energies of -0.46 and -0.54 eV, respectively. While pattern **C** had a higher adsorption energy of -0.92 eV, with two benzene rings of molecule **1** nearly parallel to the triazine rings of the corrugated $C_3N_4$ surface. In addition, the distances between oxygen and carbon atoms were about 2.60 and 2.73 Å respectively for patterns **A** and **B** (Figure S6a and S6b), indicating a physical adsorption mode of this kind of interaction. For the adsorption pattern **C**, distances of ~3.2–3.9 Å between benzene rings and triazine rings (Figure S6c) was in the range for π-π stacking interactions. As reported, π-π interactions between the electron rich $C_3N_4$ and some

aromatic molecules contribute to the molecule activation,[64-65] which may also promote further charge transfer between them and the transformation of lignin aromatic structures in this work.

In addition, we have conducted the control experiments using lignin models with *tert*-butyl substituted arenes (model **S1** and **S2**). The conversions were lower compared to that of model **1** after reaction, and yields of benzaldehyde and benzoic acid as the representative cleaved products also decreased significantly (Figure S7). Lignin models with *tert*-butyl substituted arenes might hardly take part in the most favorable interaction pattern with catalyst surface, which implies the contribution and importance of surface interaction pattern for the cleavage of reactants in this system.

**Reaction mechanism investigations**

To explore the reaction routes, we conducted several control experiments (Scheme 2). Benzaldehyde as one cleaved product could be oxidized to benzoic acid under reaction conditions (Eq. 1), leading to a mixture of them after the reaction of molecule **1**. Experiment with phenyl formate as the substrate (Eq. 2) indicated that it was relatively stable under reaction conditions, without considerable hydrolysis to phenol and HCOOH as reported[31]. Moreover, the ketone **2** was partly cleaved at the $C_\alpha$–$C_\beta$ bond with low yields of products (Eq. 3), indicating that **2** is not the intermediate during the transformation of **1**. Therefore, two routes including benzylic alcohol oxidation and oxidative $C_\alpha$–$C_\beta$ bond cleavage may co-exist during the reaction. Besides, this reaction was greatly inhibited by TEMPO (2,2,6,6-tetramethyl-1-piperidinyloxy) (Eq. 4), indicating that the reaction proceeds through certain radical intermediates.
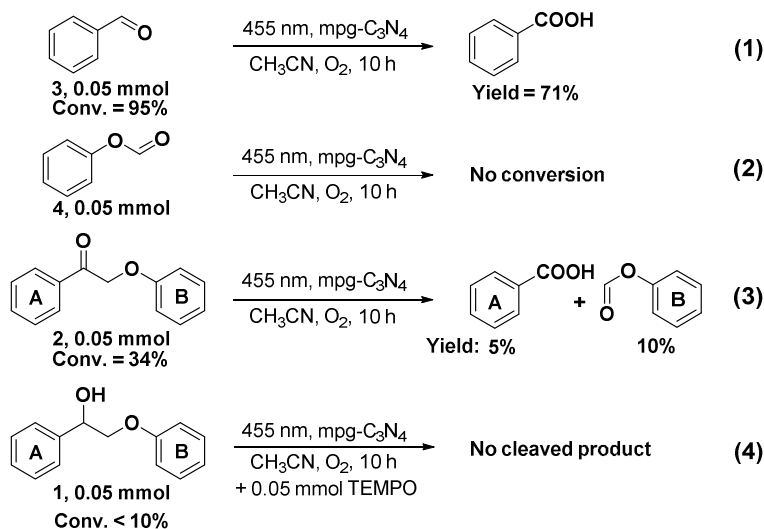
**Scheme 2.** Control experiments
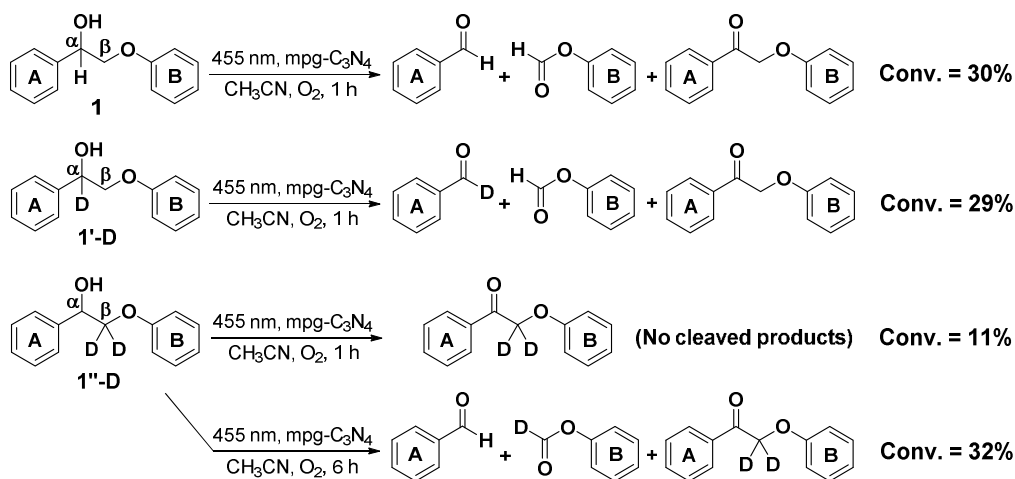


**Scheme 3.** Control experiments with deuterated substrates

In further experiments with deuterated substrates (Scheme 3), the conversion (29%) of **1'-D** with $C_\alpha$–D was close to that of substrate **1** (30%), meaning that the hydrogen abstraction of $C_\alpha$–H is not the rate-determining step during the reaction process. Meanwhile, the conversion of **1''-D** with $C_\beta$–D apparently decreased compared with that of **1,** and the generation of cleaved products was slowed down, indicating that oxidation of $C_\beta$–H is pivotal for the substrate transformation and $C_\alpha$–$C_\beta$ bond cleavage process. Moreover, the presence of $C_\alpha$–D and $C_\beta$–D in deuterated

aldehyde and phenyl formate separately (Figure S8 and S9) indicates a possible reaction mechanism shown below.
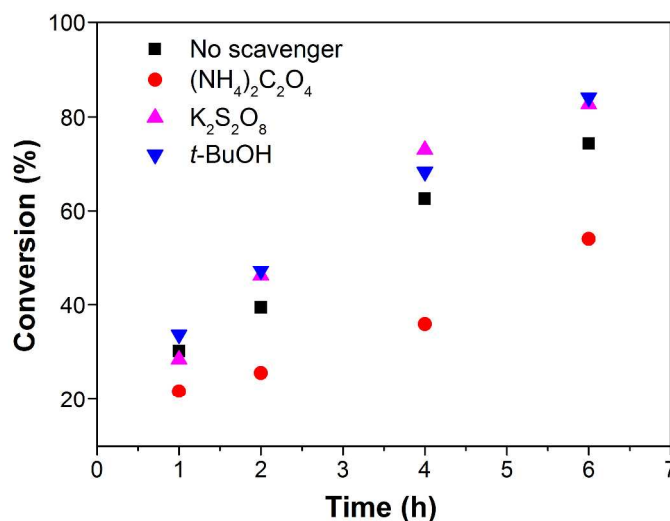


**Figure 6.** Conversion of **1** using mpg-$C_3N_4$ with different scavengers. Reaction conditions: 0.05 mmol of substrate **1**, 10 mg of mpg-$C_3N_4$, 1 mL of $CH_3CN$, 0.05 mmol of the scavenger, $O_2$ (1 atm), 455 nm LED (6 W).

To identify the active species that orient this photocatalytic reaction, $K_2S_2O_8$, $(NH_4)_2C_2O_4$, *p*-benzoquinone *(p*-BQ) and *t*-BuOH were adopted as the scavengers for photogenerated electrons, photogenerated holes, $O_2^{\bullet-}$ and $^\bullet OH$, respectively (Figure 6).[66-67] Addition of *p*-BQ improved the substrate conversion (Figure S10), as *p*-BQ itself could induce part oxidation and dissociation of the model substrate as reported before.[30] Meanwhile, $K_2S_2O_8$ or *t*-BuOH had little suppression effect on the substrate conversion, indicating that photogenerated electrons and $^\bullet OH$ radicals contribute little in this transformation. Besides, the non-promotional effect on the initial substrate conversion rate through increasing the $O_2$ pressure (Figure S11), as well as the little suppression effect of electron scavengers, also excludes that $O_2$ is initially activated and subsequently induces the substrate transformation, as $O_2^{\bullet-}$ comes from the reduction of $O_2$ by

photogenerated electrons in the conduction band of the catalyst. By contrast, addition of

$(NH_4)_2C_2O_4$ apparently inhibited the substrate conversion, revealing that photogenerated holes in

the valance band of mpg-$C_3N_4$ are main active species for the transformation of lignin model **1**.
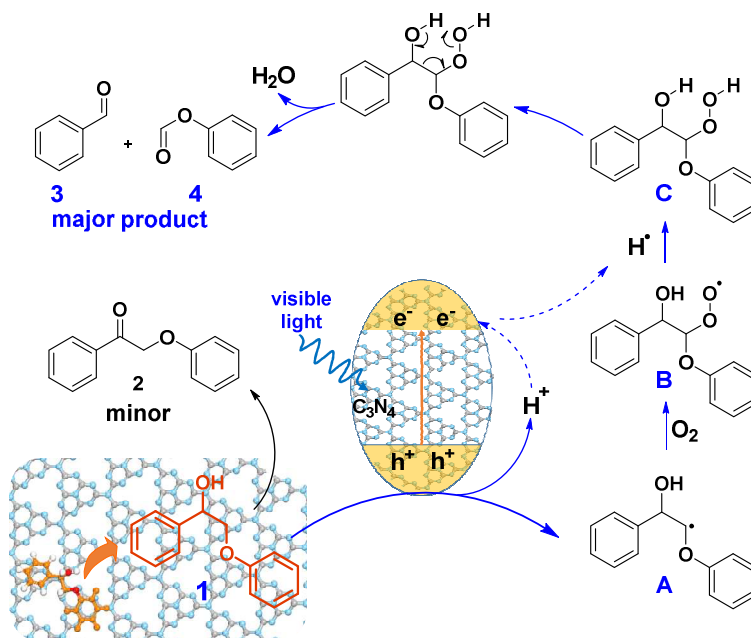


**Scheme 4.** Proposed mechanism of mpg-$C_3N_4$ catalyzed transformation of molecule **1**
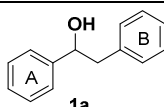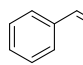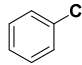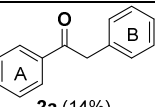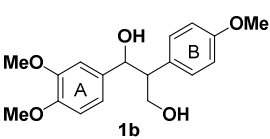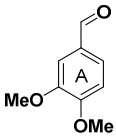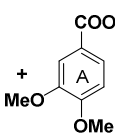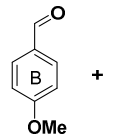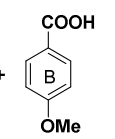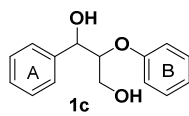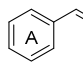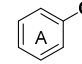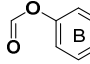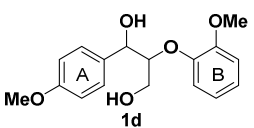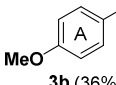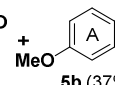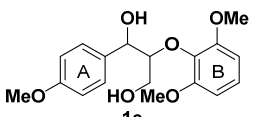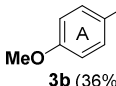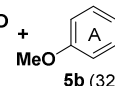
Based on the above results, we proposed a possible mechanism of photo-driven transformation

of lignin molecule **1** with mpg-$C_3N_4$ as the catalyst (Scheme 4). mpg-$C_3N_4$ is firstly excited by

visible light irradiation, generating holes and electrons separately in the valence and conduction

band. For the reactant molecule interacting with mpg-$C_3N_4$ surface, a hydrogen from $C_\beta$ is

abstracted under the role of photogenerated holes and surface basic sites on mpg-$C_3N_4$,

generating a $C_\beta$-centered radical (**A**),[33] which further combines with $O_2$ and hydrogen to give a

peroxide intermediate **C**. The following electron transfer in **C** through a six-membered ring

transition state would induce the $C_\alpha$–$C_\beta$ and O–O bond cleavage, forming aromatic aldehyde and
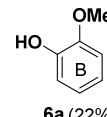
phenyl formate as the major products. Part of the aldehyde product can be further oxidized to

benzoic acid. On the other side, photogenerated electrons can also reduce $O_2$ molecules to the

superoxide radical anion $O_2^{\bullet-}$, which would deprotonate benzylic alcohol to the alkoxide anion

and finally result in the formation of by-product **2**.[41]

**Oxidative cleavage of other lignin models**

We then tested the applicability of mpg-C$_3$N$_4$ for visible light driven transformations of other

lignin models (Table 3). β-1 lignin models like 1,2-diphenylethanol (**1a**) and **1b** were also

dissociated, with aromatic aldehydes and acids as the major cleaved products. Besides, other

β-O-4 linkages with C$_\gamma$−OH (**1c-1e**) could also yield cleaved products under the same conditions.

Yields of phenolic part (with benzene ring **B**) with more methoxy groups were low due to the

overoxidation or polymerization of phenolic compounds or intermediates under light irradiation,

which would be problematic for hardwood lignins that mainly contain syringyl units.

**Table 3.** Oxidative cleavage of typical lignin models catalyzed by mpg-C$_3$N$_4$ under visible light [a]



| Substrate | Time | Conversion (%) | Main Products (Yield, %) [b] |
|---|---|---|---|
| **1a** | 10 h | 89% | **3** (54%) + **5** (12%) + **2a** (14%) |
| **1b** | 8 h | > 98% | **3a** (60%) + **5a** (27%) + **3b** (64%) + **5b** (25%) |
| **1c** | 12 h | > 98% | **3** (53%) + **5** (37%) + **4** (40%) |
| **1d** | 10 h | > 98% | **3b** (36%) + **5b** (37%) + **6a** (22%) |
| **1e** | 10 h | > 98% | **3b** (36%) + **5b** (32%) |

[a] Reaction conditions: 0.05 mmol of lignin model, 10 mg of mpg-C$_3$N$_4$, 1 mL of CH$_3$CN, O$_2$ (1

atm), 455 nm LED light (6 W). [b] For the reaction of **1a**, yield of **3** (**5**) = $\dfrac{\text{moles of product } \mathbf{3}\,(\mathbf{5}) \text{ obtained}}{\text{moles of substrate } \mathbf{1a} \text{ input}}$

$\times \frac{1}{2} \times 100\%$, yield of **2a** $= \frac{\text{moles of product } \mathbf{2a} \text{ obtained}}{\text{moles of substrate } \mathbf{1a} \text{ input}} \times 100\%$. Unless otherwise specified, yields of

other products were calculated as the molar ratio of the corresponding product to the substrate

input.

In addition, recycle experiments of model **1** using mpg-$C_3N_4$ were conducted, with the

catalyst showing relatively stable activity after four cycles (Figure S12). Moreover, a large scale

reaction was also conducted using a xenon illuminator by magnifying the reaction system

(Figure S13), achieving a 90% conversion of substrate **1** after 20 h and considerable amounts of

cleaved products (see the SI for details), which indicates the potential application of this

photocatalytic system. However, photocatalytic transformation of real lignin may be hampered

by its dark brown color and low solubility, which limit the light absorption by a photocatalyst.[68]

We performed a control experiment of model **1** in the presence of sodium lignosulfonate (Figure

S14), which resulted in a much lower conversion (from 96% to 43%) and less products after 10 h.

To address potential difficulties of visible light photocatalysis with real lignin extracts, using

some newly developed photocatalytic reactors with flow systems[69-70], improving the solubility of

lignin, and reducing lignin color via UV irradiation first[71-73] may be helpful to improve the light

throughput and reaction efficiency.

**CONCLUSIONS**

In conclusion, a mild one-step photocatalytic strategy has been developed for C–C bond

cleavage of lignin models using a mesoporous graphitic carbon nitride photocatalyst. β-O-4 and

β-1 linkages were effectively cleaved into aromatic aldehydes (acids) and phenolic esters.

Solid-state NMR experiments identified the spatial proximity of aromatic hydrogens from model

molecule and the $NH_x$ groups on mpg-$C_3N_4$, with DFT calculations revealing the favorable π-π

stacking interactions between them. Photogenerated holes were primarily active for the substrate transformation, according to the trapping experiments and mechanism studies. This study may shed light on the hole-induced direct conversion of lignin linkages on a solid catalyst surface and inspire further development of visible-light-driven heterogeneous catalysts for lignin conversion.

**Supporting Information**

Quantification methods of the reaction, supplementary experimental results and discussion, procedures of synthesizing different lignin models, NMR data and spectra

**ACKNOWLEDGMENT**

**REFERENCES**

(1) Zakzeski, J.; Bruijnincx, P. C. A.; Jongerius, A. L.; Weckhuysen, B. M. The Catalytic Valorization of Lignin for the Production of Renewable Chemicals. *Chem. Rev.* **2010**, *110*, 3552-3599.

(2) Li, C.; Zhao, X.; Wang, A.; Huber, G. W.; Zhang, T. Catalytic Transformation of Lignin for the Production of Chemicals and Fuels. *Chem. Rev.* **2015**, *115*, 11559-11624.

(3) Karkas, M. D.; Matsuura, B. S.; Monos, T. M.; Magallanes, G.; Stephenson, C. R. J. Transition-metal catalyzed valorization of lignin: the key to a sustainable carbon-neutral future. *Org. Biomol. Chem.* **2016**, *14*, 1853-1914.

(4) Deuss, P. J.; Barta, K. From models to lignin: Transition metal catalysis for selective bond cleavage reactions. *Coord. Chem. Rev.* **2016**, *306*, 510-532.

(5) Van den Bosch, S.; Schutyser, W.; Vanholme, R.; Driessen, T.; Koelewijn, S. F.; Renders, T.; De Meester, B.; Huijgen, W. J. J.; Dehaen, W.; Courtin, C. M.; Lagrain, B.; Boerjan, W.; Sels, B. F. Reductive lignocellulose fractionation into soluble lignin-derived phenolic monomers and dimers and processable carbohydrate pulps. *Energy Environ. Sci.* **2015**, *8*, 1748-1763.

(6) Xia, Q. N.; Chen, Z. J.; Shao, Y.; Gong, X. Q.; Wang, H. F.; Liu, X. H.; Parker, S. F.; Han, X.; Yang, S. H.; Wang, Y. Q. Direct hydrodeoxygenation of raw woody biomass into liquid alkanes. *Nat. Commun.* **2016**, *7*, 11162-11171.

(7) Xia, Q.; Cuan, Q.; Liu, X.; Gong, X.; Lu, G.; Wang, Y. Pd/NbOPO$_4$ Multifunctional Catalyst for the Direct Production of Liquid Alkanes from Aldol Adducts of Furans. *Angew. Chem. Int. Ed.* **2014**, *53*, 9755-9760.

(8) Nichols, J. M.; Bishop, L. M.; Bergman, R. G.; Ellman, J. A. Catalytic C−O Bond Cleavage of 2-Aryloxy-1-arylethanols and Its Application to the Depolymerization of Lignin-Related Polymers. *J. Am. Chem. Soc.* **2010**, *132*, 12554-12555.

(9) Sedai, B.; Díaz-Urrutia, C.; Baker, R. T.; Wu, R.; Silks, L. A. P.; Hanson, S. K. Aerobic Oxidation of β-1 Lignin Model Compounds with Copper and Oxovanadium Catalysts. *ACS Catal.* **2013**, *3*, 3111-3122.

(10) Sedai, B.; Díaz-Urrutia, C.; Baker, R. T.; Wu, R.; Silks, L. A. P.; Hanson, S. K. Comparison of Copper and Vanadium Homogeneous Catalysts for Aerobic Oxidation of Lignin Models. *ACS Catal.* **2011**, *1*, 794-804.

(11) Galkin, M. V.; Smit, A. T.; Subbotina, E.; Artemenko, K. A.; Bergquist, J.; Huijgen, W. J. J.; Samec, J. S. M. Hydrogen-free catalytic fractionation of woody biomass. *ChemSusChem* **2016**, *9*, 3280-3287.

(12) Son, S.; Toste, F. D. Non-Oxidative Vanadium-Catalyzed C−O Bond Cleavage: Application to Degradation of Lignin Model Compounds. *Angew. Chem. Int. Ed.* **2010**, *49*, 3791-3794.

(13) Mottweiler, J.; Rinesch, T.; Besson, C.; Buendia, J.; Bolm, C. Iron-catalysed oxidative cleavage of lignin and β-O-4 lignin model compounds with peroxides in DMSO. *Green Chem.* **2015**, *17*, 5001-5008.

(14) Jiang, Y.; Yan, L.; Yu, H.; Zhang, Q.; Fu, Y. Mechanism of Vanadium-Catalyzed Selective C–O and C–C Cleavage of Lignin Model Compound. *ACS Catal.* **2016**, *6*, 4399-4410.

(15) Song, Q.; Wang, F.; Cai, J.; Wang, Y.; Zhang, J.; Yu, W.; Xu, J. Lignin depolymerization (LDP) in alcohol over nickel-based catalysts via a fragmentation–hydrogenolysis process. *Energy & Environmental Science* **2013**, *6*, 994.

(16) Mottweiler, J.; Puche, M.; Rauber, C.; Schmidt, T.; Concepcion, P.; Corma, A.; Bolm, C. Copper- and Vanadium-Catalyzed Oxidative Cleavage of Lignin using Dioxygen. *ChemSusChem* **2015**, *8*, 2106-2113.

(17) Wang, M.; Lu, J. M.; Li, L. H.; Li, H. J.; Liu, H. F.; Wang, F. Oxidative C(OH)C bond cleavage of secondary alcohols to acids over a copper catalyst with molecular oxygen as the oxidant. *J. Catal.* **2017**, *348*, 160-167.

(18) Hanson, S. K.; Baker, R. T. Knocking on wood: base metal complexes as catalysts for selective oxidation of lignin models and extracts. *Acc. Chem. Res.* **2015**, *48*, 2037-2048.

(19) Zhou, Z. Z.; Liu, M. X.; Li, C. J. Selective Copper–N-Heterocyclic Carbene (Copper-NHC)-Catalyzed Aerobic Cleavage of β-1 Lignin Models to Aldehydes. *ACS Catal.* **2017**, *7*, 3344-3348.

(20) Liu, H. F.; Wang, M.; Li, H. J.; Luo, N. C.; Xu, S. T.; Wang, F. New protocol of copper-catalyzed oxidative C(CO)C bond cleavage of aryl and aliphatic ketones to organic acids using $O_2$ as the terminal oxidant. *J. Catal.* **2017**, *346*, 170-179.

(21) Wang, M.; Lu, J. M.; Zhang, X. C.; Li, L. H.; Li, H. J.; Luo, N. C.; Wang, F. Two-Step, Catalytic C–C Bond Oxidative Cleavage Process Converts Lignin Models and Extracts to Aromatic Acids. *ACS Catal.* **2016**, *6*, 6086-6090.

(22) Zhang, C. F.; Wang, F. Sell a dummy: Adjacent functional group modification strategy for the catalytic cleavage of lignin β-O-4 linkage. *Chin. J. Catal.* **2017**, *38*, 1102-1107.

(23) Parthasarathi, R.; Romero, R. A.; Redondo, A.; Gnanakaran, S. Theoretical Study of the Remarkably Diverse Linkages in Lignin. *J. Phys. Chem. Lett.* **2011**, *2*, 2660-2666.

(24) Kim, S.; Chmely, S. C.; Nimlos, M. R.; Bomble, Y. J.; Foust, T. D.; Paton, R. S.; Beckham, G. T. Computational Study of Bond Dissociation Enthalpies for a Large Range of Native and Modified Lignins. *J. Phys. Chem. Lett.* **2011**, *2*, 2846-2852.

(25) Nguyen, J. D.; Matsuura, B. S.; Stephenson, C. R. J. A Photochemical Strategy for Lignin Degradation at Room Temperature. *J. Am. Chem. Soc.* **2014**, *136*, 1218-1221.

(26) Kärkäs, M. D.; Bosque, I.; Matsuura, B. S.; Stephenson, C. R. J. Photocatalytic Oxidation of Lignin Model Systems by Merging Visible-Light Photoredox and Palladium Catalysis. *Org. Lett.* **2016**, *18*, 5166-5169.

(27) Luo, N. C.; Wang, M.; Li, H. J.; Zhang, J.; Hou, T. T.; Chen, H. J.; Zhang, X. C.; Lu, J. M.; Wang, F. Visible-Light-Driven Self-Hydrogen Transfer Hydrogenolysis of Lignin Models and Extracts into Phenolic Products. *ACS Catal.* **2017**, *7*, 4571-4580.

(28) Luo, N. C.; Wang, M.; Li, H. J.; Zhang, J.; Liu, H. F.; Wang, F. Photocatalytic Oxidation–Hydrogenolysis of Lignin β-O-4 Models via a Dual Light Wavelength Switching Strategy. *ACS Catal.* **2016**, *6*, 7716-7721.

(29) Luo, J.; Zhang, X.; Lu, J.; Zhang, J. Fine Tuning the Redox Potentials of Carbazolic Porous Organic Frameworks for Visible-Light Photoredox Catalytic Degradation of Lignin β-O-4 Models. *ACS Catal.* **2017**, *7*, 5062-5070.

(30) Mitchell, L. J.; Moody, C. J. Solar Photochemical Oxidation of Alcohols using Catalytic Hydroquinone and Copper Nanoparticles under Oxygen: Oxidative Cleavage of Lignin Models. *J. Org. Chem.* **2014**, *79*, 11091-11100.

(31) Gazi, S.; Ng, W. K. H.; Ganguly, R.; Moeljadi, A. M. P.; Hirao, H.; Sen Soo, H. Selective photocatalytic C−C bond cleavage under ambient conditions with earth abundant vanadium complexes. *Chem. Sci.* **2015**, *6*, 7130-7142.

(32) Gazi, S.; Dokic, M.; Moeljadi, A. M. P.; Ganguly, R.; Hirao, H.; Soo, H. S. Kinetics and DFT Studies of Photoredox Carbon-Carbon Bond Cleavage Reactions by Molecular Vanadium Catalysts under Ambient Conditions. *ACS Catal.* **2017**, *7*, 4682-4691.

(33) Hou, T. T.; Luo, N. C.; Li, H. J.; Heggen, M.; Lu, J. M.; Wang, Y. H.; Wang, F. Yin and Yang Dual Characters of CuOx Clusters for C−C Bond Oxidation Driven by Visible Light. *ACS Catal.* **2017**, *7*, 3850-3859.

(34) Masih, D.; Ma, Y.; Rohani, S. Graphitic $C_3N_4$ based noble-metal-free photocatalyst systems: A review. *Appl. Catal. B* **2017**, *206*, 556-588.

(35) Ong, W. J.; Tan, L. L.; Ng, Y. H.; Yong, S. T.; Chai, S. P. Graphitic Carbon Nitride (g-$C_3N_4$)-Based Photocatalysts for Artificial Photosynthesis and Environmental Remediation: Are We a Step Closer To Achieving Sustainability? *Chem. Rev.* **2016**, *116*, 7159-7329.

(36) Zhao, Z.; Sun, Y.; Dong, F. Graphitic carbon nitride based nanocomposites: a review. *Nanoscale* **2015**, *7*, 15-37.

(37) Gong, Y.; Li, M.; Li, H.; Wang, Y. Graphitic carbon nitride polymers: promising catalysts or catalyst supports for heterogeneous oxidation and hydrogenation. *Green Chem.* **2015**, *17*, 715-736.

(38) Chen, Y.; Zhang, J.; Zhang, M.; Wang, X. Molecular and textural engineering of conjugated carbon nitride catalysts for selective oxidation of alcohols with visible light. *Chem. Sci.* **2013**, *4*, 3244.

(39) Wang, X.; Blechert, S.; Antonietti, M. Polymeric Graphitic Carbon Nitride for Heterogeneous Photocatalysis. *ACS Catal.* **2012**, *2*, 1596-1606.

(40) Su, F.; Mathew, S. C.; Möhlmann, L.; Antonietti, M.; Wang, X.; Blechert, S. Aerobic Oxidative Coupling of Amines by Carbon Nitride Photocatalysis with Visible Light. *Angew. Chem. Int. Ed.* **2011**, *50*, 657-660.

(41) Su, F.; Mathew, S. C.; Lipner, G.; Fu, X.; Antonietti, M.; Blechert, S.; Wang, X. mpg-$C_3N_4$-Catalyzed Selective Oxidation of Alcohols Using $O_2$ and Visible Light. *J. Am. Chem. Soc.* **2010**, *132*, 16299-16301.

(42) Chen, Y.; Wang, B.; Lin, S.; Zhang, Y.; Wang, X. Activation of n → π* Transitions in Two-Dimensional Conjugated Polymers for Visible Light Photocatalysis. *J. Phys. Chem. C* **2014**, *118*, 29981-29989.

(43) Shi, L.; Liang, L.; Wang, F. X.; Liu, M. S.; Chen, K. L.; Sun, K. N.; Zhang, N. Q.; Sun, J. M. Higher Yield Urea-Derived Polymeric Graphitic Carbon Nitride with Mesoporous Structure and Superior Visible-Light-Responsive Activity. *ACS Sustainable Chem. Eng.* **2015**, *3*, 3412-3419.

(44) Zhang, Y. H.; Zhang, N.; Tang, Z. R.; Xu, Y. J. Identification of $Bi_2WO_6$ as a highly selective visible-light photocatalyst toward oxidation of glycerol to dihydroxyacetone in water. *Chem. Sci.* **2013**, *4*, 1820-1824.

(45) Kresse, G.; Furthmüller, J. Efficiency of ab-initio total energy calculations for metals and semiconductors using a plane-wave basis set. *Comp. Mater. Sci.* **1996**, *6*, 15-50.

(46) Kresse, G.; Furthmüller, J. Efficient iterative schemes for ab initio total-energy calculations using a plane-wave basis set. *Phys. Rev. B* **1996**, *54*, 11169-11186.

(47) Perdew, J. P.; Burke, K.; Ernzerhof, M. Generalized Gradient Approximation Made Simple. *Phys. Rev. Lett.* **1996**, *77*, 3865-3868.

(48) Kresse, G.; Joubert, D. From ultrasoft pseudopotentials to the projector augmented-wave method. *Phys. Rev. B* **1999**, *59*, 1758-1775.

(49) Blöchl, P. E. Projector augmented-wave method. *Phys. Rev. B* **1994**, *50*, 17953-17979.

(50) Jagadeesh, R. V.; Stemmler, T.; Surkus, A.-E.; Junge, H.; Junge, K.; Beller, M. Hydrogenation using iron oxide–based nanocatalysts for the synthesis of amines. *Nat. Protocols* **2015**, *10*, 548-557.

(51) Wang, M.; Li, L. H.; Lu, J. M.; Li, H. J.; Zhang, X. C.; Liu, H. F.; Luo, N. C.; Wang, F. Acid promoted C–C bond oxidative cleavage of β-O-4 and β-1 lignin models to esters over a copper catalyst. *Green Chem.* **2017**, *19*, 702-706.

(52) Lan, H. C.; Li, L. L.; An, X. Q.; Liu, F.; Chen, C. B.; Liu, H. J.; Qu, J. H. Microstructure of

carbon nitride affecting synergetic photocatalytic activity: Hydrogen bonds vs. structural defects.

*Appl. Catal. B* **2017**, *204*, 49-57.

(53) Shalom, M.; Inal, S.; Neher, D.; Antonietti, M. $SiO_2$/carbon nitride composite materials: The

role of surfaces for enhanced photocatalysis. *Catal. Today* **2014**, *225*, 185-190.

(54) Thomas, A.; Fischer, A.; Goettmann, F.; Antonietti, M.; Muller, J.-O.; Schlogl, R.; Carlsson,

J. M. Graphitic carbon nitride materials: variation of structure and morphology and their use as

metal-free catalysts. *J. Mater. Chem.* **2008**, *18*, 4893-4908.

(55) Holst, J. R.; Gillan, E. G. From Triazines to Heptazines: Deciphering the Local Structure of

Amorphous Nitrogen-Rich Carbon Nitride Materials. *J. Am. Chem. Soc.* **2008**, *130*, 7373-7379.

(56) Kang, Y.; Yang, Y.; Yin, L.; Kang, X.; Wang, L.; Liu, G.; Cheng, H. Selective Breaking of

Hydrogen Bonds of Layered Carbon Nitride for Visible Light Photocatalysis. *Adv. Mater.* **2016**,

*28*, 6471-6477.

(57) Wang, Y.; Yao, J.; Li, H.; Su, D.; Antonietti, M. Highly selective hydrogenation of phenol

and derivatives over a Pd@carbon nitride catalyst in aqueous media. *J. Am. Chem. Soc.* **2011**, *133*,

2362-2365.

(58) An, J.; Zhang, G.; Zheng, R.; Wang, P. Removing lignin model pollutants with

$BiFeO_3$-g-$C_3N_4$ compound as an efficient visible-light-heterogeneous Fenton-like catalyst. *J.

Environ. Sci.* **2016**, *48*, 218-229.

(59) Lotsch, B. V.; Doeblinger, M.; Sehnert, J.; Seyfarth, L.; Senker, J.; Oeckler, O.; Schnick, W.

Unmasking melon by a complementary approach employing electron diffraction, solid-state NMR

spectroscopy, and theoretical calculations-structural characterization of a carbon nitride polymer.

*Chem. Eur. J.* **2007**, *13*, 4969-4980.

(60) Jürgens, B.; Irran, E.; Senker, J.; Kroll, P.; Müller, H.; Schnick, W. Melem (2,5,8-Triamino-tri-s-triazine), an Important Intermediate during Condensation of Melamine Rings to Graphitic Carbon Nitride: Synthesis, Structure Determination by X-ray Powder Diffractometry, Solid-State NMR, and Theoretical Studies. *J. Am. Chem. Soc.* **2003**, *125*, 10288-10300.

(61) Brown, S. P.; Spiess, H. W. Advanced Solid-State NMR Methods for the Elucidation of Structure and Dynamics of Molecular, Macromolecular, and Supramolecular Systems. *Chem. Rev.* **2001**, *101*, 4125-4156.

(62) Liu, F.; Feng, N.; Wang, Q.; Xu, J.; Qi, G.; Wang, C.; Deng, F. Transfer Channel of Photoinduced Holes on a $TiO_2$ Surface As Revealed by Solid-State Nuclear Magnetic Resonance and Electron Spin Resonance Spectroscopy. *J. Am. Chem. Soc.* **2017**, *139*, 10020-10028.

(63) Azofra, L. M.; MacFarlane, D. R.; Sun, C. A DFT study of planar vs. corrugated graphene-like carbon nitride (g-$C_3N_4$) and its role in the catalytic performance of $CO_2$ conversion. *Phys. Chem. Chem. Phys.* **2016**, *18*, 18507-18514.

(64) Goettmann, F.; Fischer, A.; Antonietti, M.; Thomas, A. Chemical Synthesis of Mesoporous Carbon Nitrides Using Hard Templates and Their Use as a Metal-Free Catalyst for Friedel–Crafts Reaction of Benzene. *Angew. Chem. Int. Ed.* **2006**, *45*, 4467-4471.

(65) Ji, J.; Wen, J.; Shen, Y.; Lv, Y.; Chen, Y.; Liu, S.; Ma, H.; Zhang, Y. Simultaneous Noncovalent Modification and Exfoliation of 2D Carbon Nitride for Enhanced Electrochemiluminescent Biosensing. *J. Am. Chem. Soc.* **2017**, *139*, 11698-11701.

(66) Raja, P.; Bozzi, A.; Mansilla, H.; Kiwi, J. Evidence for superoxide-radical anion, singlet oxygen and OH-radical intervention during the degradation of the lignin model compound

(3-methoxy-4-hydroxyphenylmethylcarbinol). *J. Photochem. Photobiol. A: Chem.* **2005**, *169*, 271-278.

(67) Li, W.; Li, D.; Lin, Y.; Wang, P.; Chen, W.; Fu, X.; Shao, Y. Evidence for the Active Species Involved in the Photodegradation Process of Methyl Orange on TiO$_2$. *J. Phys. Chem. C* **2012**, *116*, 3552-3560.

(68) Kuehnel, M. F.; Reisner, E. Solar Hydrogen Generation from Lignocellulose. *Angew. Chem. Int. Ed.* **2018**, *57*, 2-9.

(69) Pieber, B.; Shalom, M.; Antonietti, M.; Seeberger, P. H.; Gilmore, K. Continuous Heterogeneous Photocatalysis in Serial Micro-Batch Reactors. *Angew. Chem. Int. Ed.* **2018**.

(70) Abdiaj, I.; Alcázar, J. Improving the throughput of batch photochemical reactions using flow: Dual photoredox and nickel catalysis in flow for C(sp$^2$)−C(sp$^3$) cross-coupling. *Biorg. Med. Chem.* **2017**, *25*, 6190-6196.

(71) Awungacha Lekelefac, C.; Hild, J.; Czermak, P.; Herrenbauer, M. Photocatalytic Active Coatings for Lignin Degradation in a Continuous Packed Bed Reactor. *Int.J. Photoenergy* **2014**, *2014*, 1-10.

(72) Wang, J.; Deng, Y.; Qian, Y.; Qiu, X.; Ren, Y.; Yang, D. Reduction of lignin color via one-step UV irradiation. *Green Chem.* **2016**, *18*, 695-699.

(73) Qi, Y.; Hempelmann, R.; Volmer, D. A. Shedding light on the structures of lignin compounds: photo-oxidation under artificial UV light and characterization by high resolution mass spectrometry. *Anal. Bioanal. Chem.* **2016**, *408*, 8203-8210.

**TOC**